

# UNIVERSITY OF BIRMINGHAM

## Research at Birmingham

### Number Size Distribution of Atmospheric Particles in a suburban Beijing in the Summer and Winter of 2015

Du, Peng; Gui, Huaqiao; Zhang, Jiaoshi; Liu, Jianguo; Yu, Tongzhu; Wang, Jie; Cheng, Yin; Shi, Zongbo

DOI:

[10.1016/j.atmosenv.2018.05.023](https://doi.org/10.1016/j.atmosenv.2018.05.023)

License:

Creative Commons: Attribution-NonCommercial-NoDerivs (CC BY-NC-ND)

*Document Version*

Peer reviewed version

*Citation for published version (Harvard):*

Du, P, Gui, H, Zhang, J, Liu, J, Yu, T, Wang, J, Cheng, Y & Shi, Z 2018, 'Number Size Distribution of Atmospheric Particles in a suburban Beijing in the Summer and Winter of 2015' *Atmospheric Environment*, vol. 186, pp. 32-44. <https://doi.org/10.1016/j.atmosenv.2018.05.023>

[Link to publication on Research at Birmingham portal](#)

#### **General rights**

Unless a licence is specified above, all rights (including copyright and moral rights) in this document are retained by the authors and/or the copyright holders. The express permission of the copyright holder must be obtained for any use of this material other than for purposes permitted by law.

- Users may freely distribute the URL that is used to identify this publication.
- Users may download and/or print one copy of the publication from the University of Birmingham research portal for the purpose of private study or non-commercial research.
- User may use extracts from the document in line with the concept of 'fair dealing' under the Copyright, Designs and Patents Act 1988 (?)
- Users may not further distribute the material nor use it for the purposes of commercial gain.

Where a licence is displayed above, please note the terms and conditions of the licence govern your use of this document.

When citing, please reference the published version.

#### **Take down policy**

While the University of Birmingham exercises care and attention in making items available there are rare occasions when an item has been uploaded in error or has been deemed to be commercially or otherwise sensitive.

If you believe that this is the case for this document, please contact [UBIRA@lists.bham.ac.uk](mailto:UBIRA@lists.bham.ac.uk) providing details and we will remove access to the work immediately and investigate.

# Number Size Distribution of Atmospheric Particles in a suburban Beijing in the Summer and Winter of 2015

Peng Du<sup>1,2</sup>, Huaqiao Gui<sup>1,3</sup>, Jiaoshi Zhang<sup>1\*</sup>, Jianguo Liu<sup>1,3\*</sup>, Tongzhu  
Yu<sup>1</sup>, Jie Wang<sup>1</sup>, Yin Cheng<sup>1</sup>, Zongbo Shi<sup>4</sup>

1. Key Laboratory of Environmental Optics and Technology, Anhui Institute of Optics and Fine  
Mechanics, Chinese Academy of Sciences, Hefei 230031, China

2. University of Chinese Academy of Sciences, Beijing 100049, China

3. Center for Excellence in Regional Atmospheric Environment, Institute of Urban Environment,  
Chinese Academy of Sciences, Xiamen 361021, China

4. School of Geography, Earth and Environmental Sciences, University of Birmingham,  
Edgbaston, Birmingham, B15 2TT, United Kingdom

**Abstract.** Particle number size distribution in a suburban Beijing was measured during the HOPE-J3A (Haze Observation Project Especially for Jing–Jin–Ji Area) field campaigns in 2015 from 18 June to 23 July (summer) and 2 to 25 December (winter). Average particle concentrations during the summer and winter campaigns were  $9.6\pm 4.8\times 10^3\text{cm}^{-3}$  and  $13.9\pm 8.3\times 10^3\text{cm}^{-3}$ , respectively. Particle numbers were dominated by Aitken mode particles in both seasons. During the winter campaign, pollution events occurred every four to five days, each lasting for two to three days. In contrast, pollution events lasted for one to two days every six to seven days during the summer campaign. Aitken mode particles were 50% higher in the winter but new particle formation (NPF) events occurred more frequently in the summer. NPF events usually starts at around 10:00 LT (local time) in the summer but 12:00 LT in the winter. Aitken and accumulation mode particles accounted for 43.5% and 38.2% of all particles. The proportion of Aitken mode to total particles remained almost the same during summer, while it increased as haze intensified in winter. Particle number concentration was closely correlated with traffic and residents living activities and

28 wind speed, with higher concentrations during rush hours, heating period and in the  
29 southerly wind. These results, when combined with trajectory cluster analysis, suggest  
30 that Aitken and accumulation mode particles were mainly from regional transport  
31 during the summer campaign, but from vehicle and coal-combustion emissions during  
32 the winter campaign.

33 **Key words: Particle Number Size distribution, Beijing, aerosol,**  
34 **Trajectory Cluster Analysis, New Particle Formation**

35

## 36 **1. Introduction**

37 Aerosol particles play an important role in the atmosphere because of their  
38 significant effects on air quality, visibility ([Watson, 2002](#)), direct and indirect climate  
39 forcing ([Anderson et al., 2003](#); [Andreae and Rosenfeld, 2008](#); [Bahadur et al., 2012](#);  
40 [Mahowald, 2011](#); [Ramanathan et al., 2001](#)), the environment ([Cao et al., 2013](#); [Huang](#)  
41 [et al., 2014](#)) and human health ([Nel, 2005](#); [Tang et al., 2017](#); [Zheng et al., 2014](#)).  
42 Accordingly, these particles have received a great deal of attention from the  
43 government and the general public. The rapid economic and industrial development  
44 and urbanization that have occurred in China have brought about serious  
45 environmental problems in Chinese megacities, especially in the  
46 Beijing–Tianjin–Hebei region, the Yangtze River delta, and the Pearl River delta  
47 ([Chan and Yao, 2008](#); [Gao et al., 2009](#); [Han et al., 2015](#); [Parrish and Zhu, 2009](#);  
48 [Zhuang et al., 2014](#)). As the capital of China and a rapidly developing city, Beijing  
49 has been experiencing severe haze pollution for years. Despite many measures taken  
50 by the government to address this issue ([Sun et al., 2016](#); [Tang et al., 2015](#); [Wang et](#)  
51 [al., 2010](#); [Xu et al., 2016a](#)), air pollution is not improving as rapidly as it could. The  
52 PM<sub>2.5</sub> in Beijing is still abnormally elevated, and often greatly exceeds the level of 75  
53  $\mu\text{g m}^{-3}$  considered by the China National Ambient Air Quality Standard (NAAQS) to  
54 be harmful to health ([Ji et al., 2014](#); [Xu et al., 2016b](#); [Zhang et al., 2013](#)).

55 Measurements of particle number size distributions have been conducted

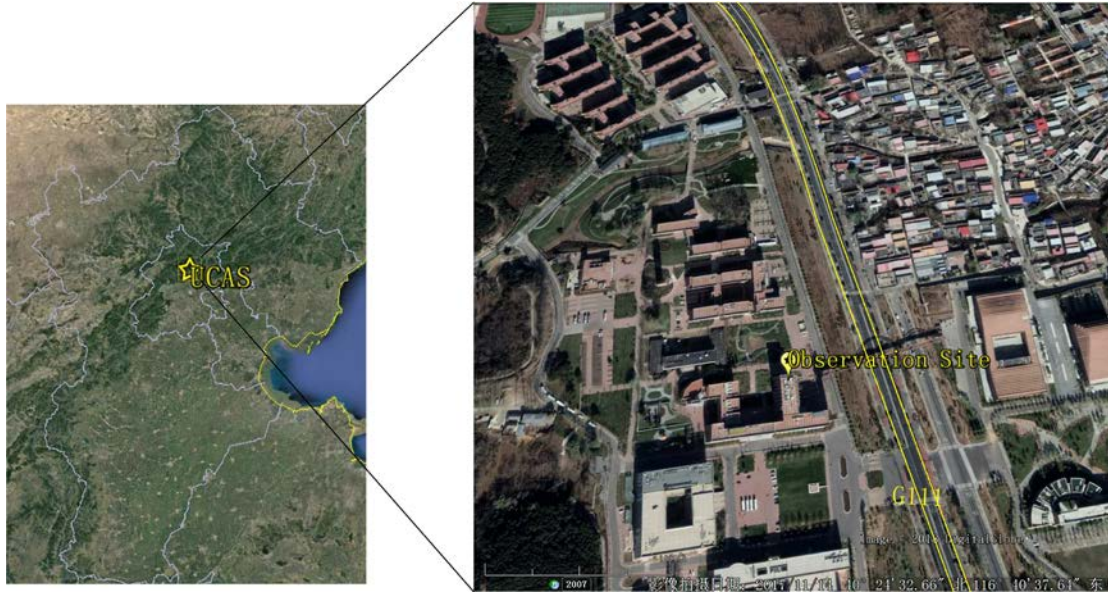
56 worldwide ([Gao et al., 2012](#); [Gao et al., 2009](#); [Hussein et al., 2004](#); [Quan et al., 2014](#);  
57 [Stanier et al., 2004](#); [Wehner and Wiedensohler, 2003](#); [Zhang et al., 2016](#)). When  
58 compared with rural areas and background areas, the concentrations of atmospheric  
59 particles in urban areas is higher (Wehner and Wiedensohler, 2003; Hussein et al.,  
60 2004). Moreover, the concentration of atmospheric particles in winter in urban areas  
61 was higher than that in summer, and the diurnal variation of atmospheric particles was  
62 significantly influenced by traffic emissions. To study the formation and evolution of  
63 atmospheric particles in Beijing, many scholars have conducted observations and  
64 experiments investigating the number concentration distribution of atmospheric  
65 aerosols. However, most of these have only focused on a pollution process or unique  
66 period ([An et al., 2007](#); [Liu et al., 2017](#); [Sun et al., 2014](#); [Tang et al., 2015](#); [Wang et](#)  
67 [al., 2010](#); [Wang et al., 2014c](#); [Xin et al., 2010](#); [Zhang et al., 2017](#)). The seasonal  
68 variation of particle number size distribution can reflect the periodic pollution process  
69 to a certain extent, such as the higher frequency of haze in winter than that in summer.  
70 The distribution of particles under different pollution conditions may demonstrate  
71 implicit links to the pollution source ([Wang et al., 2014b](#)). The new particle formation  
72 (NPF) is one of the important sources of atmospheric particles and cloud condensation  
73 nuclei. The NPF events also exhibits a regular seasonal variation ([Wu et al., 2007](#)).  
74 Studying the characteristics and mechanisms of NPF will help to further understand  
75 the climatic, environmental and health effects of atmospheric particulates. In addition,  
76 meteorological parameters such as wind direction temperature and wind speed play an  
77 important role in influencing the particle number size distribution, accounting for  
78 about 37% of all factors. Because of the typical warm temperate semi-humid  
79 continental monsoon climate, hot and rainy summer, and cold and dry winter, it had a  
80 significant impact on the distribution of particles in Beijing ([Liang et al., 2017](#);  
81 [Schäfer et al., 2013](#); [Sun et al., 2015](#)). Moreover, regional transport plays an important  
82 role in changing the particle number concentrations ([Chen et al., 2017](#); [Zhu et al.,](#)  
83 [2016](#)). The meteorological parameters could alter the size distribution of atmospheric  
84 particles, which may signify the potential sources of the particles--local emissions and  
85 regional transport.

86 Here, we report continuous measurements of the particle size distribution of  
87 aerosols at a suburban site (Huairou) during winter and summer in 2015. The  
88 influence of meteorological parameters, especially wind speed and direction, on the  
89 particle number size distributions of atmospheric aerosols was analyzed. The mixed  
90 single-particle Lagrangian integral transport and diffusion model (HYSPLIT)  
91 developed by the Ocean Resources and Atmospheric Administration (NOAA) Air  
92 Resources Laboratory (ARL) was used to simulate the trajectories of air masses  
93 reaching the observation points during summer and winter. The correlation between  
94 different mode particles and local emissions as well as regional transport were then  
95 investigated.

96

## 97 **2. Methodology**

98 The observations took place at the Yanqi Lake campus of the University of  
99 Chinese Academy of Sciences (UCAS), which is located in the Huairou District,  
100 northeastern Beijing ( $40^{\circ}24'24.45''\text{N}$ ,  $116^{\circ}40'32.95''\text{E}$ ), as shown in Figure 1. The  
101 summer campaign was from 18 June to 23 July and winter from 2 to 25 December  
102 2015. Due to the SMPS was broke down from 15 to 21 December 2015, the data for  
103 this period was missing. The Yanqi Lake Campus of the UCAS is about 50 km away  
104 from the central Beijing. The campus is located at the junction of Yanshan Mountain  
105 and the North China Plain (NCP), where northwest airflow and south air flow  
106 converge, making it easy to observe the impact of regional transport. The observation  
107 site is adjacent to China National Highway 111 and a rural residential area. The  
108 instruments were installed on the top floor of Teaching Building 1, with the sample  
109 inlet about 1.5 m above the roof.



110

111 Figure 1. The map of the North China Plain. The observation site (UCAS) is marked with yellow  
 112 balloon sign.

113 The particle number size distributions of the aerosols between 11.1 and 1083.3  
 114 nm was measured every 7 mins using a scanning mobility particle sizer (SMPS,  
 115 Grimm Aerosol Technik GmbH, Germany, Model 5.400), which consists of an  
 116 Am-241 neutralizer (Model 5.522), a long Vienna-type differential mobility analyzer  
 117 (L-DMA, model 55-990) and a condensation particle counter (CPC, model  
 118 5.403)([Heim et al., 2004](#)). The size distribution inversion was conducted using the  
 119 manufacturer-provided software (GRIMM 5.477 Version 1.35) developed and  
 120 described in detail by [Reischl \(1991\)](#). Diffusion losses and the effects of  
 121 multi-charged particles were corrected using the instrument software. The SMPS was  
 122 validated with laboratory-generated, commercially available certified (Duke Standard)  
 123 NIST-traceable monodispersed polystyrene latex (PSL) particles of two known sizes,  
 124  $203\pm 5\text{nm}$  and  $499\pm 8\text{nm}$ , before and after the campaign ([Joshi et al., 2012](#)). The  
 125 deviation between measured particle sizes and the certified diameters of the PSL  
 126 spheres agreed to within 4%. Considering the uncertainty in PSL size and other  
 127 possible experimental uncertainties, the results were well within the confidence  
 128 required to proceed further. Atmospheric aerosols were divided into nucleation mode  
 129 ( $<25\text{ nm}$ ), Aitken mode (25-100 nm), accumulation mode (0.1-1  $\mu\text{m}$ ) to calculate the  
 130 concentrations in different size categories.

131 The ambient aerosols were dried to a RH below 20% using a Nafion drier  
132 (MD-700; Perma Pure LLC), then passed into the SMPS as the sample flow. The RH  
133 of the sheath flow of SMPS was dried to below 20% using a diffusion drier, then  
134 passed through a HEPA filter before being sent to the DMA. The temperature and  
135 humidity of the sample flow and sheath flow were measured using a digital humidity  
136 and temperature sensor (SHT11; Sensirion China Co., Ltd) and logged every minute  
137 to ensure that the aerosol size distributions were measured under dry conditions;  
138 therefore, hygroscopic growth was not considered.

139 The Hybrid Single-Particle Lagrangian Integrated Trajectory (HYSPLIT) model  
140 developed by NOAA/ARL (National Oceanic and Atmospheric Administration/Air  
141 Resources Laboratory) was used to calculate the backward trajectories of air masses  
142 arriving at the observation site during summer and winter campaigns. The mode data  
143 comes from the GDAS observations of the National Environmental Prediction Center  
144 of the United States. The 36-h backward trajectories starting at 200 m were calculated  
145 every 6 hours (at 00:00, 06:00, 12:00, 18:00). Then the built-in cluster analysis tool of  
146 HYSPLIT was used to group the air mass trajectories according to the spatial total  
147 variance (TSV).

148 The meteorological parameters, including wind speed and direction, temperature,  
149 relative humidity, and atmospheric pressure, were continuously recorded by a MetPak  
150 automatic weather station (Gill Instruments Ltd., Lymington, UK). Moreover, the  
151 wind profiles from 40 to 320m were also recorded by a Doppler wind lidar (Windcube  
152 8, Leosphere, Orsay, France). The hourly average values of mass concentrations of  
153 PM<sub>2.5</sub> and pollutant gases (SO<sub>2</sub>, NO<sub>2</sub>, O<sub>3</sub>, and CO) were retrieved from the China  
154 National Environmental Monitoring Center National Urban Air Quality Real-time  
155 Release Platform (<http://113.108.142.147:20035/emcpublish>).

156

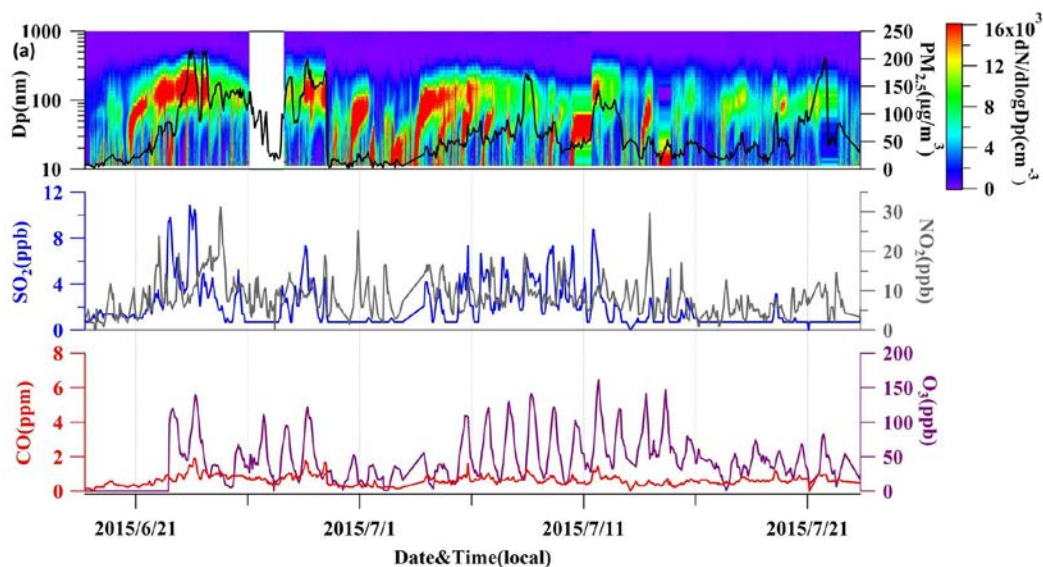
### 157 **3. Results and discussion**

#### 158 **3.1 Overview of particle number size distribution**

159 An overview of the measurement results of the aerosol size distribution, mass

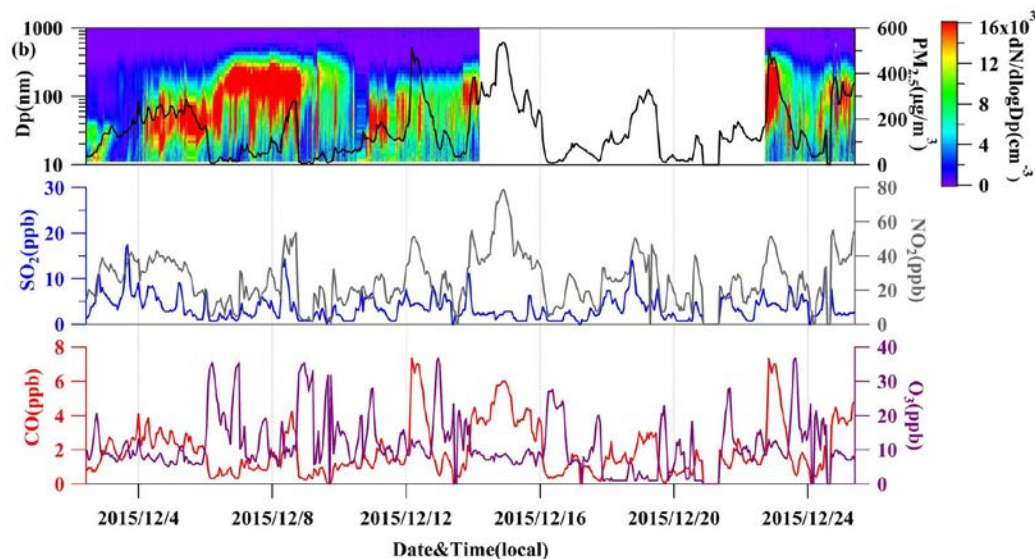


160 concentration of PM<sub>2.5</sub> and gaseous pollutants is shown in Figure 2. Particle number  
 161 concentrations showed periodic behavior, with lower concentrations being observed  
 162 in summer and higher in winter. Particle number concentrations are well correlated to  
 163 PM<sub>2.5</sub> mass concentrations. Mass concentration of PM<sub>2.5</sub> during the winter campaign  
 164 was  $122.9 \pm 123.4 \mu\text{g m}^{-3}$ , which was almost two times higher than that during the  
 165 summer campaign ( $66.4 \pm 50.2 \mu\text{g m}^{-3}$ ). Periodic pollution process was observed every  
 166 four to five days, each lasting for two to three days during the winter campaign,  
 167 whereas they only lasted for one to two days every six to seven days during the  
 168 summer campaign. The frequency of new particle formation (NPF) events was higher  
 169 during summer and subsequently accompanied by a significant growth process. Mass  
 170 concentration of PM<sub>2.5</sub> increased with the NPF and subsequent growth process. The  
 171 correlation coefficient between NO<sub>2</sub> and PM<sub>2.5</sub> was 0.75 as well as CO and PM<sub>2.5</sub>  
 172 were well correlated with 0.86, indicating a significant contribution from the primary  
 173 emissions.



174



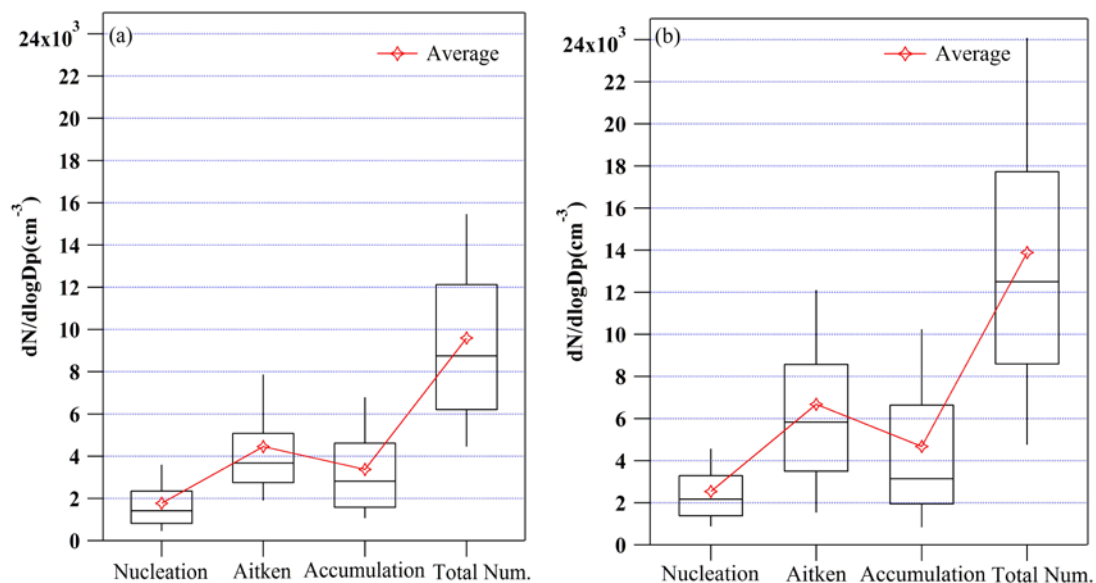


175

176 Figure 2. Time series of aerosol number size distribution measured by SMPS, mass concentrations  
 177 of PM<sub>2.5</sub> and gaseous pollutants (SO<sub>2</sub>, NO<sub>2</sub>, O<sub>3</sub>, and CO) during the summer (a) and the winter (b)  
 178 campaigns.

179 Figure 3 shows the statistical variations of particle number concentrations of  
 180 nucleation, Aitken and accumulate mode and total number concentration during the  
 181 summer and winter. Mean total number concentration of particles in the winter was  
 182  $13.9 \pm 8.3 \times 10^3 \text{ cm}^{-3}$ , which was 45% higher than that during summer ( $9.6 \pm 4.8 \times 10^3$   
 183  $\text{cm}^{-3}$ ). Aitken mode particles contributed 46% and 48% to total particle numbers in  
 184 the summer and winter, following by accumulation (35% and 34%) and nucleation  
 185 mode (19% and 18%) particles. Number concentration of Aitken mode particles were  
 186 50% higher in the winter than that in the summer, whereas nucleation and  
 187 accumulation mode particles were 43.5% and 38.2% higher.

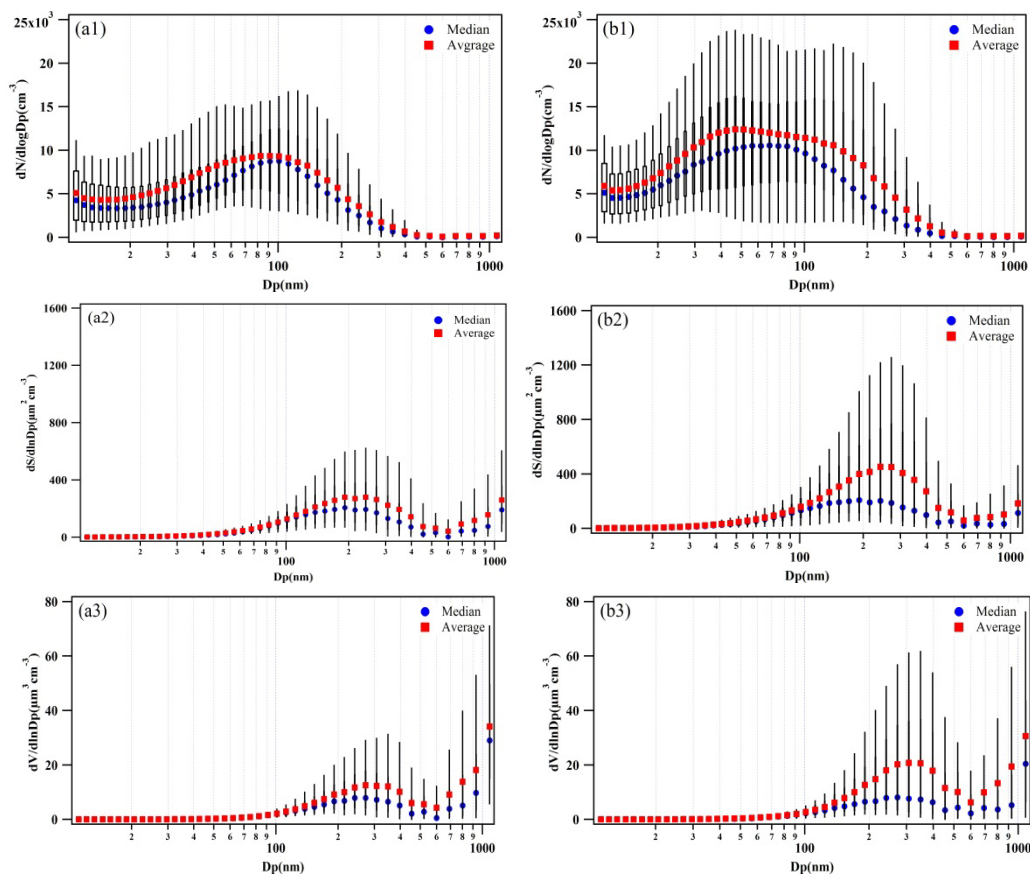
188



189

190 Figure 3. Box plots showing the statistical variations of particle number concentrations  
 191 during the summer (a) and the winter (b).

192 Figure 4 shows the statistical variations in the size, surface area and volume  
 193 distributions of particles below 1  $\mu\text{m}$  at the Huairou site during the summer and  
 194 winter of 2015. More than 99.5% of the particles are below 500 nm; Accumulation  
 195 mode particles in the range of 100–500 nm made a significant contribution to the total  
 196 surface area and volume. Furthermore, a significant  $>1 \mu\text{m}$  coarse mode in the volume  
 197 was also observed. We also observed a peak between 100 and 200 nm in the winter  
 198 and the summer, which has comparable average number concentrations. A significant  
 199 peak between 40 and 50 nm was also seen during the winter, with an even higher  
 200 number concentration than that between 100–200 nm. Since the number concentration  
 201 of the Aitken mode particles is affected by the primary emissions from transportation  
 202 sources (Liu et al., 2017), it can be concluded that the observation site is more affected  
 203 by local primary emission in the winter. The residence time of large particles is  
 204 usually short, and they are easily removed by dry and wet sedimentation, so the  
 205 concentration of particles beyond 500 nm is similar during winter and summer. The  
 206 peak values of surface area concentration and volume concentration during the  
 207 summer and the winter were similar, between 200–300 nm and 300 nm, respectively,  
 208 but the concentrations in the winter were much higher than that in the summer.



209

210

211

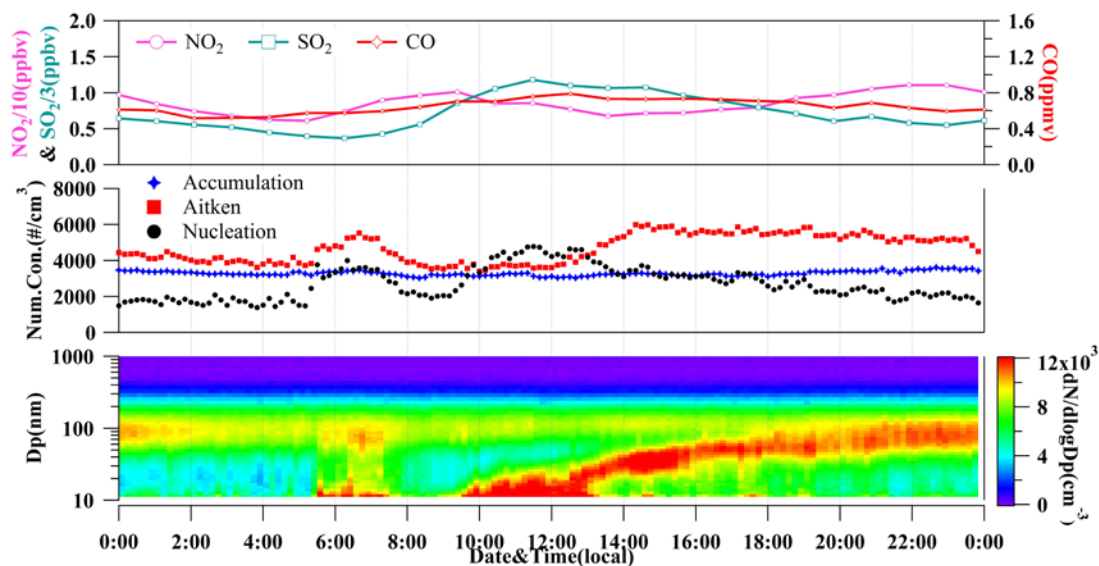
212 Figure 4. Box plots showing the particle number size distribution observed during the summer and  
 213 the winter (a1, b1); and the size distribution of surface area (a2, b2) and volume (a3, b3)  
 214 calculated from the number size distribution.

215

### 216 3.2 Diurnal variations of particle number size distributions

217 Figures 5 and 7 show the average diurnal variation of number size distributions  
 218 of total, and nucleation, Aitken and accumulation mode particles during the two  
 219 campaigns. Many factors influence the diurnal variation of the particle number size  
 220 distributions, including the formation of secondary particles, local primary emissions,  
 221 and meteorological conditions ([Liu et al., 2016](#); [Shen et al., 2011](#); [Wu et al., 2008](#)).  
 222 The SO<sub>2</sub> concentration tended to increase as the nucleation mode particles, which  
 223 indicated that the formation of secondary particles was the main contributor to the  
 224 concentration of nucleation mode particles ([Gao et al., 2012](#); [Sun et al., 2016](#); [Wang](#)  
 225 [et al., 2013](#); [Yue et al., 2009](#)). The newly formed particles can grow through  
 226 condensation and collision to Aitken mode even accumulation mode particles ([Zhang](#)  
 227 [et al., 2017](#)). Motor vehicle exhaust, coal-combustion and other primary sources also

228 contribute to particle number concentrations ([Liu et al., 2017](#); [Wu et al., 2008](#)).



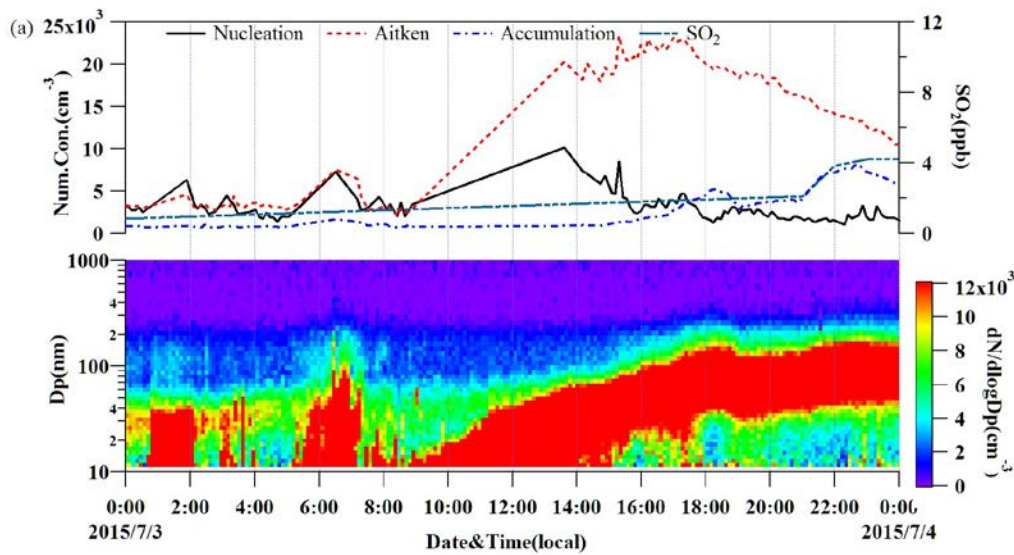
229

230 Figure 5. Average diurnal variation of NO<sub>2</sub>, SO<sub>2</sub>, CO concentrations and number size distributions  
231 of particles observed during the summer campaign.

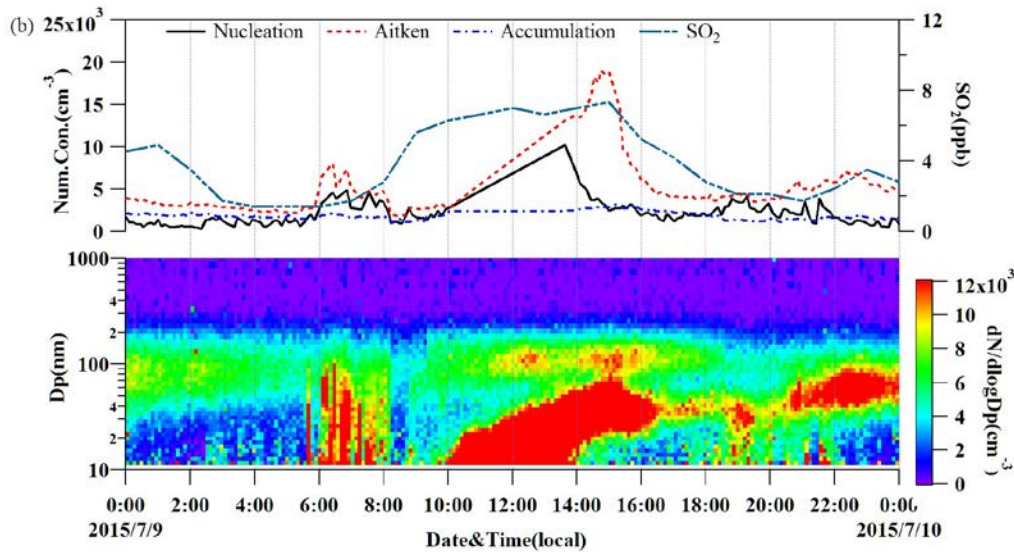
232 Figure 5 shows that there is a significant increase in the average number  
233 concentration of particles, mainly in the nucleation and Aitken mode, in the morning  
234 from 6:00 to 8:00 h during the summer campaign; meanwhile, the NO<sub>2</sub> concentration  
235 increased, which was probably caused by motor vehicle exhaust emissions during  
236 morning rush hour ([Wang et al., 2014c](#); [Wu et al., 2008](#)). After the morning peak, the  
237 concentration of nucleation and Aitken mode particles decreased to a level similar to  
238 those before the morning peak. From about 10:00 h onwards, the concentration of  
239 nucleation mode particles began to increase sharply, while that of the Aitken mode  
240 particles remained at a similar level. When the newly formed particles grew, the  
241 concentration of nucleation mode particles began to decrease, whereas that of the  
242 Aitken mode particles increased rapidly. Because the atmospheric nucleation process  
243 usually lasts for several hours, the increase in the concentration of particles in Aitken  
244 mode usually lagged behind that of nucleation mode particles ([Kulmala, 2003](#);  
245 [Kulmala et al., 2013](#); [Kulmala et al., 2007](#)). Following NPF, the particle size growth  
246 continued until the night, reaching about 80 nm, after which the concentration  
247 decreased. The NPF showed a “banana shape” in the diurnal variation of the particle  
248 number size distributions ([Gao et al., 2012](#)). Over the 36-day summer campaign, there

249 were 13 NPF events.

250 Figure 6 shows two typical NPF events during the summer campaign. The events  
251 were observed on July 3 and 9, 2015, and lasted for a few hours. The temporal  
252 developments of concentration of SO<sub>2</sub> and particle number size distributions during  
253 the NPF events were shown in Fig. 6. In the observed NPF events, the concentration  
254 of nucleation mode particles began to increase sharply at about 10:00 h with the high  
255 concentration of SO<sub>2</sub>, especially in July 9, 2015. When the newly formed particles  
256 grew, the concentration of nucleation mode particles began to decrease, whereas that  
257 of the Aitken mode particles continued to increase a period of time.



258



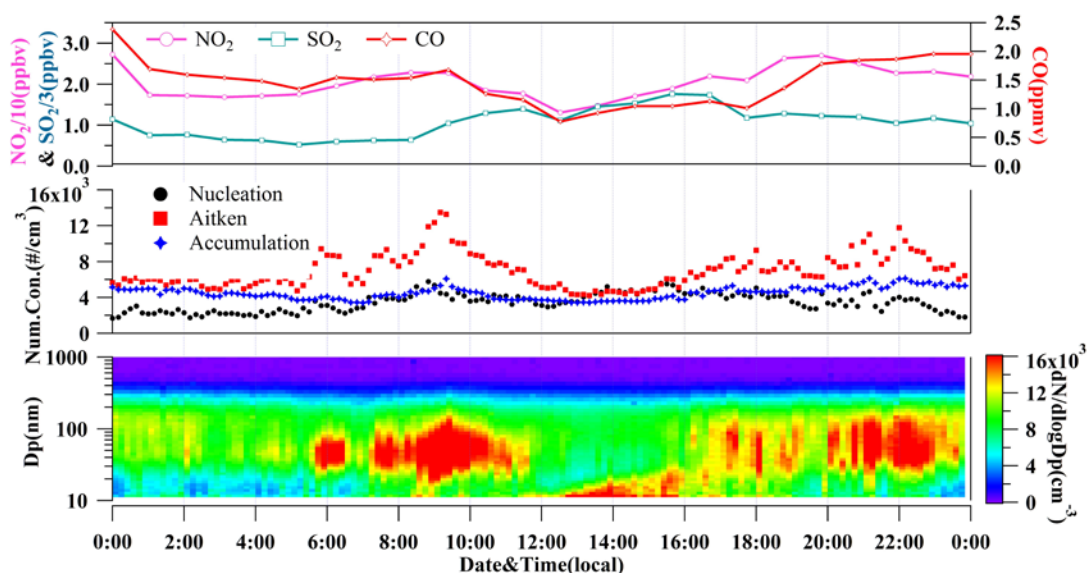
259

260 Figure 6. Time series of mass concentrations of SO<sub>2</sub>, number concentrations nucleation mode,  
261 Aitken mode particles, accumulation mode particles and image plot of particle number size



262 distributions during the two typical NPF events observed on July 3 (a) and 9 (b), 2015.

263 The concentration of particles in nucleation and Aitken mode vary greatly during  
264 the day, but this is not the case for accumulation mode particles. The concentration of  
265 nucleation mode particles was relatively low during the nighttime (19:00 h to 6:00 h),  
266 approaching  $2.0 \times 10^3 \text{ cm}^{-3}$ , while it reached as high as  $5.0 \times 10^3 \text{ cm}^{-3}$  during the NPF  
267 period. The lowest concentration of Aitken mode particles was observed before and  
268 during the occurrence of NPF episodes, which usually occurred under clean air  
269 conditions (Huang et al., 2017). Number concentration of Aitken mode particles was  
270 at their lowest level between 8:00 and 10:00 h, which was less than  $4.0 \times 10^3 \text{ cm}^{-3}$ . This  
271 might be induced by the development of the boundary layer, which leads to a dilution  
272 of air pollutants and a decrease in the concentration of atmospheric background  
273 particles (Liu et al., 2017). The newly formed particles grew continuously from  
274 nucleation to Aitken mode size, with a sharp decrease in the number concentration of  
275 Aitken mode particles, and the highest concentration reaching  $6.0 \times 10^3 \text{ cm}^{-3}$ . The  
276 accumulation mode particles were less affected by the primary emissions, and the  
277 concentration varied little in the day, remaining at about  $6.0 \times 10^3 \text{ cm}^{-3}$ .



278

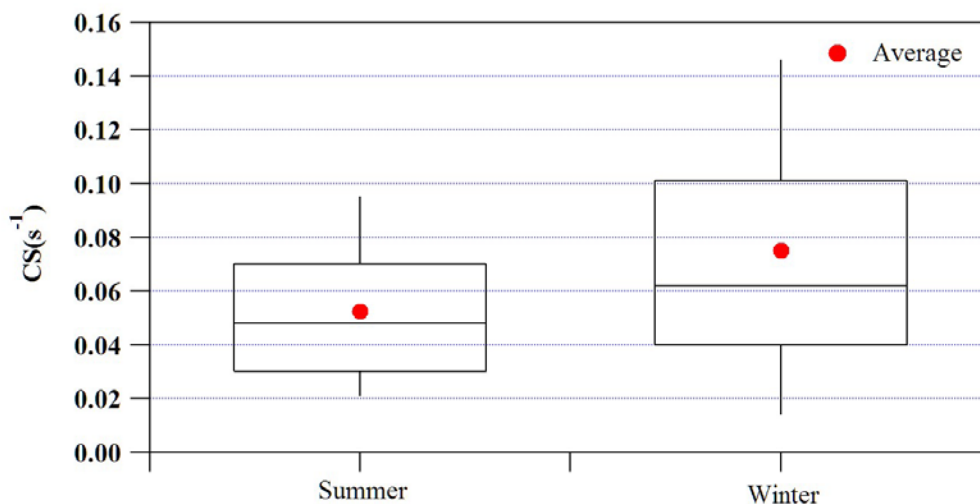
279 Figure 7. Average diurnal variation of NO<sub>2</sub>, SO<sub>2</sub>, CO concentrations and number size distributions  
280 of particles observed during the winter campaign.

281 Average number concentration of particles was very low from midnight to 6:00  
282 am during the winter campaign, but that of the nucleation mode particles was similar

283 to that in the summer (approx.  $2.0 \times 10^3 \text{ cm}^{-3}$ ). Similar to the summer morning peak, the  
284 concentration of Aitken mode particles increased rapidly at about 6:00 h in the winter  
285 and remained high until 11:30 h, when the maximum concentration was close to  
286  $1.2 \times 10^4 \text{ cm}^{-3}$ . In the meantime, the number concentrations of accumulation and  
287 nucleation mode particles also increased significantly. The concentrations of all  
288 particles were then quickly restored to a very low level after the episode.

289 Five NPF events were observed but more likely to occur in the midday (from  
290 12:00 h), with no significant increase in particle size, which may be related to the  
291 weak photochemical reaction intensity and low condensable vapor concentration in  
292 winter ([Cheung et al., 2013](#); [Wang et al., 2014a](#)). The higher the coagulation sink (CS),  
293 the less suitable for the generation and growth of new particles ([Lehtinen et al., 2003](#);  
294 [Pirjola et al., 1999](#)). Preexisting particles can scavenge newly formed particles and  
295 condensable vapors, thus suppress NPF. The CS in winter is generally higher than  
296 summer, as shown in Figure 8. This probably be another reason why the occurrence of  
297 NPF events in winter was much less than events in summer. During the NPF events,  
298 the particle number concentration in nucleation mode increased rapidly from  
299  $3.0 \times 10^3 \text{ cm}^{-3}$  to near  $5.0 \times 10^3 \text{ cm}^{-3}$ , but the period of subsequent particle growth was  
300 relatively short. It terminated at about 16:00 h when the mean size grew to about 30  
301 nm. The variation in particle number concentration from 16:00 to 20:00 h may be  
302 related to the increase in the vehicle flow during evening rush hours ([Wang et al.,](#)  
303 [2014c](#); [Wu et al., 2008](#)). From 20:00 h until midnight, the particle number size  
304 distributions appeared to be similar to that at 6:00 to 11:30 h. During the night, the  
305 concentration of CO was higher than that during the daytime. The northeast of the  
306 observation site is a residential area, where the residents still mainly rely on coal-fired  
307 heating, so the particle number size distributions appeared to have a longer duration of  
308 Aitken mode particles, which was likely because of local coal-fired emissions.





309

310 Figure 8. Box plots showing the CS during the summer and winter campaigns.

311

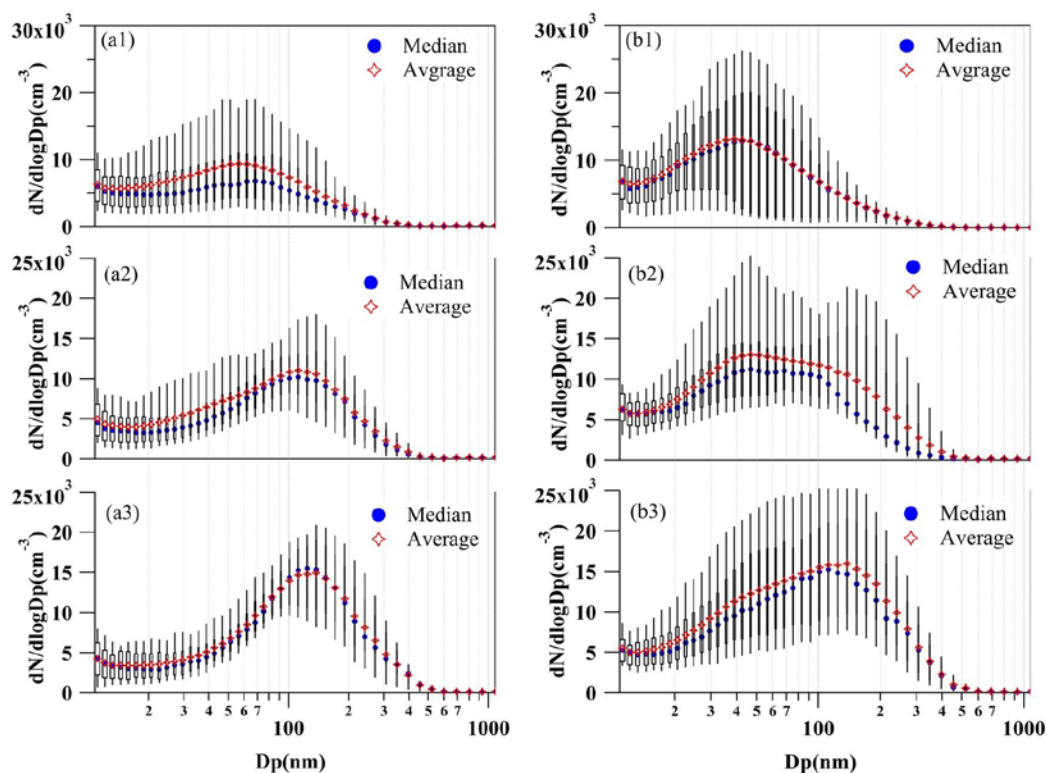
312 The diurnal variation in the particle number size distributions during winter was  
 313 somewhat similar to that in summer. The particle number concentration in the winter  
 314 ( $1.5 \times 10^4 \text{ cm}^{-3}$ ) was higher than that in the summer. The Aitken mode particles were  
 315 most abundant (52.2%), followed by accumulation mode (36.4%) and nucleation  
 316 mode (29.6%). The main sources of Aitken mode particles are the efficient growth of  
 317 nucleation mode particles and the primary emission of Aitken mode particles ([Shi et](#)  
 318 [al., 2007](#); [Yue et al., 2009](#)). However, the concentration of nucleation particles during  
 319 winter was only 30% higher than that in summer, indicating that the concentration of  
 320 the primary emission Aitken particles during winter is higher than that in summer, and  
 321 there results were consistent with the winter coal-fired heating, biomass burning and  
 322 other human activities ([Liu et al., 2017](#)).

323

### 324 3.3 Characteristics of particle number size distributions under different pollution 325 conditions

326 To further understand the variation of particle number size distributions under  
 327 different stages of hazes, pollution conditions were into three categories: 1)  
 328  $\text{PM}_{2.5} < 50 \mu\text{g m}^{-3}$ , 2)  $50 \leq \text{PM}_{2.5} \leq 100 \mu\text{g m}^{-3}$ , and 3)  $\text{PM}_{2.5} > 100 \mu\text{g m}^{-3}$ , representing three  
 329 stages of the haze evolution processes – pre-haze (clean), haze formation, and haze,

330 respectively. Statistical variations of particle number size distributions of aerosols in  
 331 the summer and the winter under different pollution conditions is shown in Figure 9.  
 332 There is a shift in size distribution towards larger sizes when haze intensifies, which  
 333 was also observed in Shaihai ([Wang et al., 2014b](#)). Regardless of the pollution  
 334 conditions, the concentration of particles in each size segment during the winter was  
 335 significantly higher than that in summer, especially for particles of <50 nm. The  
 336 concentrations of particles <50 nm in the three stages duration in the winter were  
 337  $6.7 \times 10^3 \text{ cm}^{-3}$ ,  $5.8 \times 10^3 \text{ cm}^{-3}$  and  $5.4 \times 10^3 \text{ cm}^{-3}$ , respectively, which were 46%, 54% and  
 338 98% higher than those during the summer. During the haze duration periods,  
 339 concentrations of particles <50 nm in winter were almost twice those during the  
 340 summer. The main reason for this phenomenon may be the winter traffic in the  
 341 surrounding areas and residential coal-fired and other emissions making a high  
 342 contribution to the concentrations of particles in Aitken mode ([Liu et al., 2017](#)).  
 343 Particle number size distributions during the winter haze formation stage and the  
 344 hazes showed a significant peak at about 50 nm, which was probably from the  
 345 emissions of particles from surrounding areas ([Wang et al., 2014c](#)).



346  
 347 Figure 9. Box plots showing the particle number size distribution under different pollution

348 conditions during the summer and winter: (a1, b1) pre-haze (clean) stage, (a2, b2) haze  
 349 formation stage, (a3, b3) haze stage.

350 .

351 During the pre-haze stage (before haze formation), mean particle number size  
 352 distributions showed a unimodal distribution, with a peak of about 60 nm, in the  
 353 summer but about 40 nm in the winter. Accumulation mode particles contributed 23%  
 354 to total particle numbers in the summer, while only 15% in the winter, which was  
 355 possibly due to the regional transport from the southwest pathway during the summer.  
 356 Particles in the summer and winter haze formation stages showed a bimodal  
 357 distribution, with peaks at ca. 50 nm and ca. 100 nm, respectively. The difference was  
 358 that the primary peak is about 50 nm in the summer but 100 nm in the winter. In the  
 359 winter haze formation stage, the primary peak concentration was similar to that of  
 360 summer, but that of the primary peak in the winter (around 50 nm) was 48% higher  
 361 than in the summer.

362 The distribution of particle concentration during the haze events in the summer  
 363 was unimodal, with a peak between 100 and 200 nm. In contrast, it showed a bimodal  
 364 distribution during the winter hazes, with one of the peaks at 100 and 200 nm, similar  
 365 to that in the summer, and an additional peak at ca. 50 nm.

366

367 Table 1. Means of number concentrations of particles in different mode (in  $10^3 \text{ cm}^{-3}$ )  
 368 under different pollution conditions

369

		<b>Nucleation</b>	<b>Aitken</b>	<b>Accumulation</b>	<b>Total Num.</b>
<b>Summer</b>	PM <sub>2.5</sub> <50	2.3±1.5	4.8±3.8	2.1±1.4	9.2±5.5
	50≤PM <sub>2.5</sub> ≤100	1.8±1.2	4.7±2.3	3.9±1.9	10.4±4.3
	PM <sub>2.5</sub> >100	1.4±0.8	3.9±1.2	5.5±2.3	10.8±3.2
<b>Winter</b>	PM <sub>2.5</sub> <50	3.2±1.6	6.5±4.7	1.7±1.2	11.4±6.9
	50≤PM <sub>2.5</sub> ≤100	2.6±0.7	6.6±2.9	3.0±1.6	12.2±4.1
	PM <sub>2.5</sub> >100	2.3±1.1	7.1±3.9	7.2±3.6	16.7±7.5

370

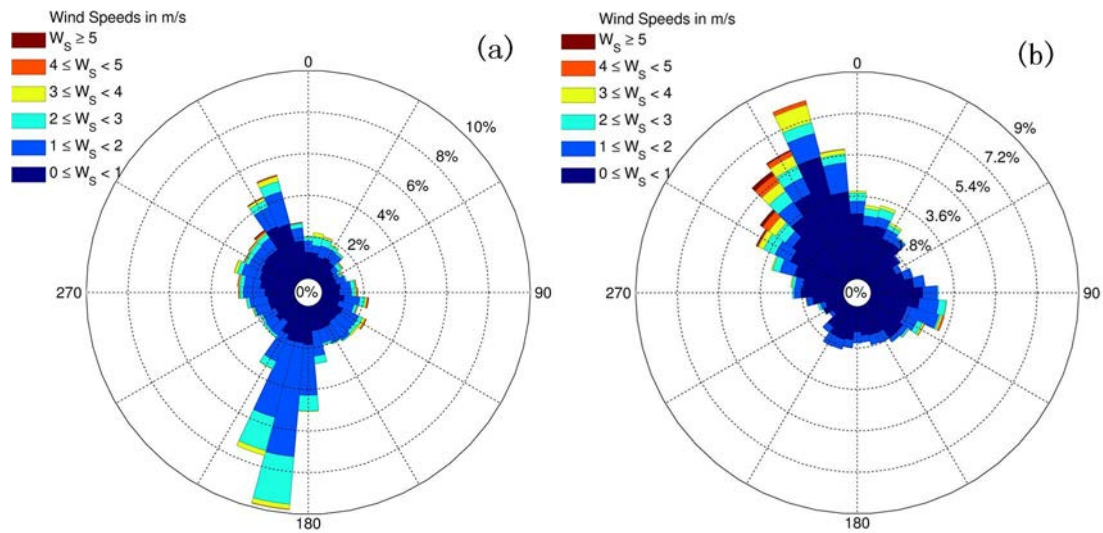
371 Table 1 showed that the difference in the total concentration of particles was not  
372 significant at different stages of typical haze events in the summer, but the proportion  
373 of each mode of particles changed substantially. The concentration of nucleation  
374 mode particles during the pre-haze stage was the highest, while it decreased  
375 significantly when the haze started to form. The varieties of particle concentration in  
376 Aitken mode were similar to those of the nucleation mode particles, while the  
377 accumulation mode particles were just the opposite. The total concentration of  
378 particles during the pre-haze stage and the haze formation stage in the winter were  
379 similar, while it increased greatly during the hazy period. Unlike in summer, the  
380 number concentration of Aitken mode particles in winter increased gradually as the  
381 haze started to form. The number concentration of nucleation mode and Aitken mode  
382 particles in the winter was generally higher than that in the same stage of summer,  
383 while the accumulation mode particles in the winter pre-haze stage and the haze  
384 formation stage was lower than those in the summer.

385 In summary, the size distribution towards larger sizes when haze intensifies  
386 during the both campaigns. In the three instances, particles in Aitken mode was  
387 highest for pre-haze and haze formation stage, while accumulation mode particles  
388 were predominant for haze stage.

389

### 390 **3.4 Effects of meteorological conditions on particle number size distributions**

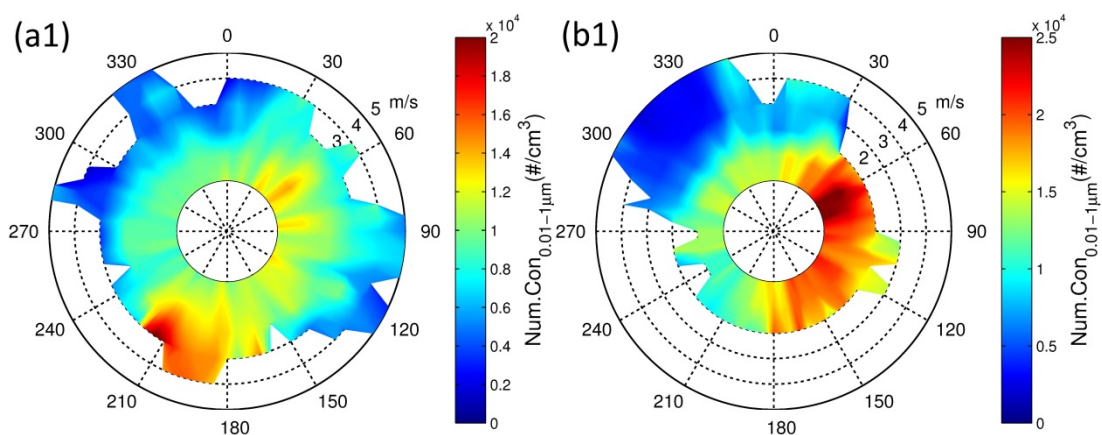
391 Figure 10 shows the frequency of mean wind direction and speed from 40 to  
392 320m in the summer and winter in Beijing. The observation site was located in the  
393 south of Yanshan Mountain, where southwest wind with a low wind speed prevails in  
394 summer, while northeast wind prevails during winter. Moreover, the air mass from the  
395 northwest is often accompanied by strong near ground wind speed, so the frequency  
396 of high wind speed during winter is relatively high.



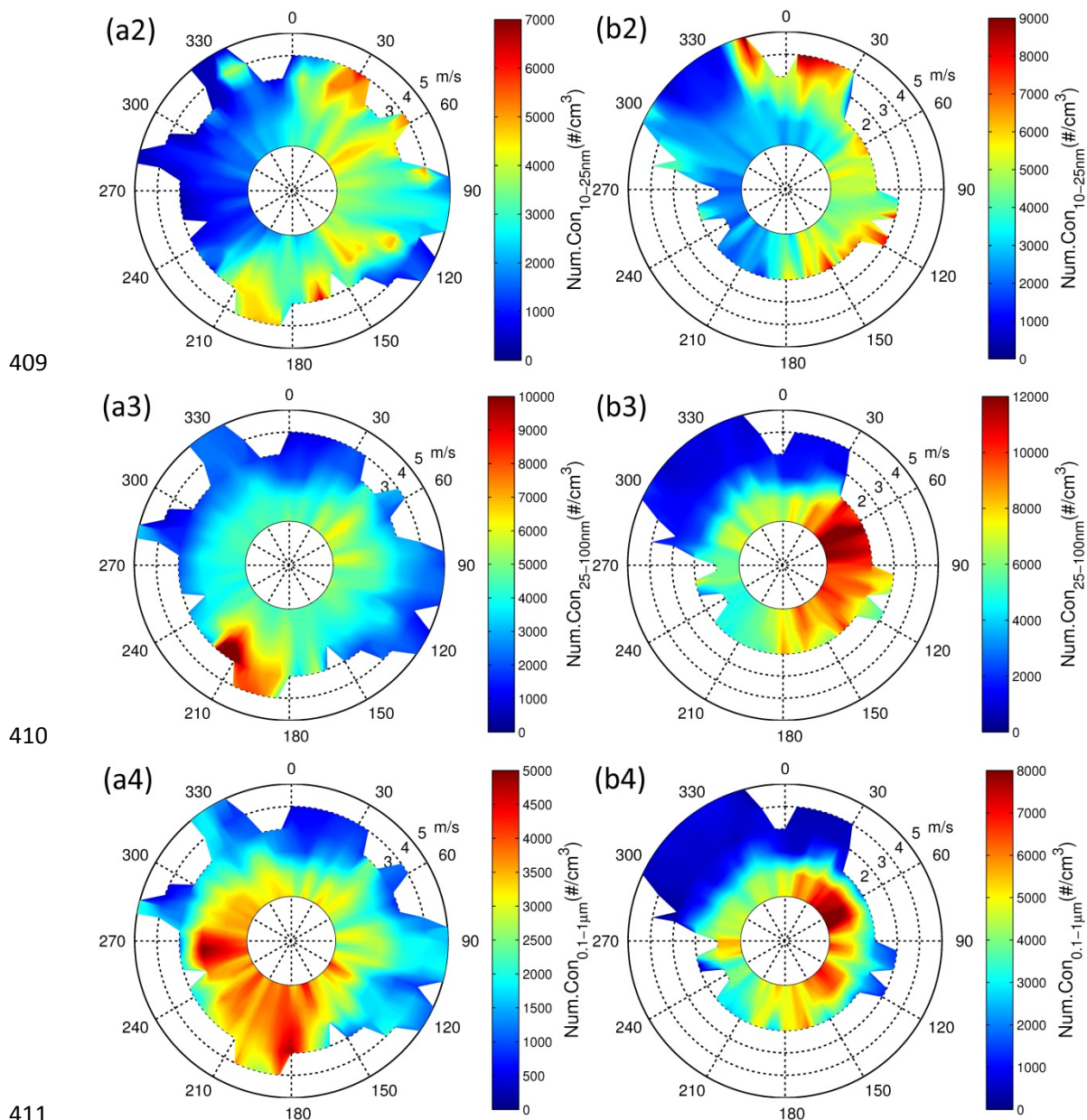
397

398 Figure 10. Mean wind direction frequency in summer (a) and winter (b) in Beijing 2015.

399 Figure 11 shows that concentration of particles was higher when the wind is from  
 400 the south than that from the north during campaigns, especially at higher wind speeds  
 401 (e.g., > 3 m/s). This is consistent with the concentration distribution characteristics of  
 402 particles in the Beijing area (Liang et al., 2017; Wu et al., 2016; Zhang et al., 2017).  
 403 The northern region of the observation site is mountain and forest, with limited human  
 404 activities, while the southern side is in the urban area of Beijing and Hebei province.  
 405 As a result, a large number of particles from Beijing and Hebei can be transported to  
 406 the site under the southerly wind. In contrast, a sustained northerly wind may dilute  
 407 the local particle pollution.



408



409  
410  
411  
412 Figure 11. Polar plots for all particles (a1, b1), and particles in the nucleation (a2, b2), Aitken (a3,  
413 b3) and accumulation mode (a4, b4) during the summer and the winter, respectively.

414 Overall, the total concentration of particles in the summer was significantly  
415 lower than that in the winter, especially when the wind is from the northeast and  
416 southeast. However, there was no significant increase in the total concentration of  
417 particles when the wind is from the southwest. Due to the surrounding environment,  
418 the site is mainly influenced by mobile sources of vehicle emission on China National  
419 Highway 111 and stationary sources from the rural settlement across the highway. In  
420 addition, the air flow coming from the southern urban areas may bring anthropogenic  
421 emissions.



422 The heights of the mixing layer in the summer has a stronger effect on the  
423 dilution of particle concentration ([Liu et al., 2017](#)), which reduces the influence of  
424 traffic emissions to a certain extent. During the winter heating period, the  
425 coal-combustion activities of the nearby residential area are frequent. The  
426 concentration of CO during winter campaign was agreed with the PM<sub>2.5</sub> with R<sup>2</sup> was  
427 0.86, and more than two times higher than that of summer, which led to a significant  
428 increase in the particle concentration of local emissions. These results suggest that the  
429 observation site is mainly affected by local emissions during the winter, but by  
430 regional transport through the southwest pathway in the summer.

431 The high particle concentrations in nucleation mode mainly occurred when the  
432 wind is from the north at high wind speed during both campaigns. However, when the  
433 concentration of nucleation mode particles was high, the corresponding  
434 concentrations of Aitken mode and accumulation mode were very low. These findings  
435 indicate that the northerly wind with high speed brought in clean air and plays a  
436 positive role in dilution and diffusion of the local particles, promoting NPF events.

437 The number concentration distribution of Aitken mode particles in the summer  
438 was significantly higher under strong southwesterly, indicating that the regional  
439 transport through the southwest passage made a large contribution to the  
440 concentration of the Aitken mode particles at the study site. The sporadic high  
441 concentration of particles under the low wind speeds when the air is from the  
442 northeast may be affected by local traffic emissions ([Shi et al., 2007](#)). The  
443 accumulation mode particles in the summer were higher when the wind is from the  
444 west and south with little difference between low and high wind speeds. This suggests  
445 that local emissions and regional transport both contributed to the concentration of  
446 particles in the accumulation mode.

447 The concentration of Aitken mode particles in the winter was higher primarily  
448 when the wind speed is low. It was significantly higher when the wind is from the east,  
449 which might be from the contribution from the local traffic and the coal-combustion  
450 emissions in the winter. At the same time, the concentration of accumulation mode  
451 particles was higher when the wind is from the northwest than those from the east and

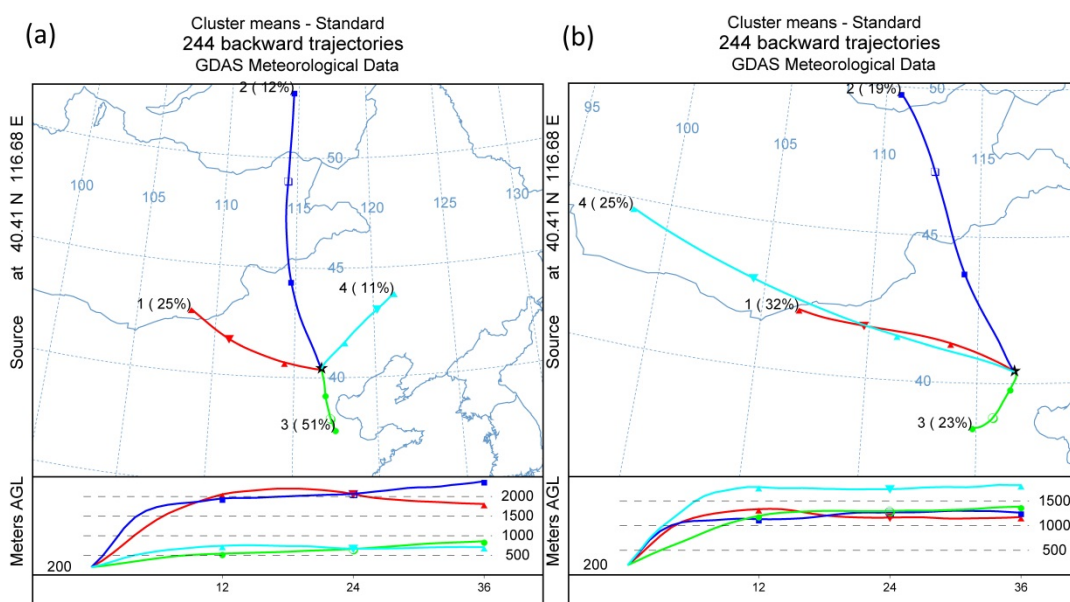


452 southwest. Considering that the coal combustion process is more likely to produce  
 453 accumulation mode particles ([Liu et al., 2016](#); [Zhang et al., 2011](#)), it can be inferred  
 454 that the residential coal-combustion in the northeast of the observation site may be a  
 455 more importance source than traffic.

456

### 457 3.5 Air mass backward trajectory clusters

458 The back trajectories differed significantly between summer and winter - a  
 459 majority of the air masses came from the south in the summer but from the west and  
 460 northwest in the winter ([Zhang et al., 2013](#)), as shown in Figure 12.



461

462 Figure 12. The 36 h back trajectories starting at 200 m above ground level in the observation site  
 463 were calculated every 6 h (at 00:00, 06:00, 12:00, and 18:00 local time) during summer (a) and  
 464 winter (b) in 2015.

465 The trajectories of air masses arriving at the observation site in the summer and  
 466 winter can be divided into four categories or clusters: northwestern (NW),  
 467 southwestern (including southern, SW), northern (N), and northeastern (NE)  
 468 directions. Table 2 summarizes the percentage of each trajectory cluster in the winter  
 469 and summer, as well as the origin and the average number concentration of each mode  
 470 of particles and the total concentration corresponding to each trajectory cluster.

471

472 Table 2. The percentage and origin of each trajectory cluster and means (with one

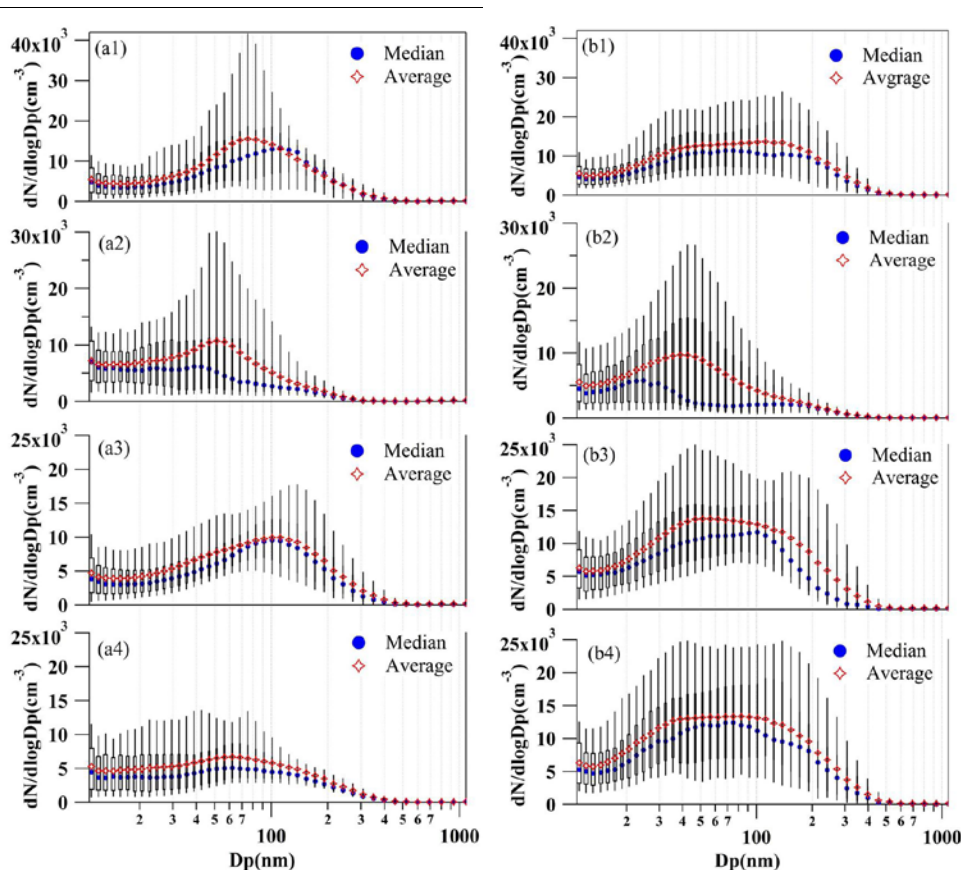
473 standard deviation) of number concentrations of particles in each mode and total  
 474 number concentration ( $10^3 \text{ cm}^{-3}$ ) during summer and winter  
 475

		<b>Percent</b>	<b>Origin</b>	<b>Nucleation</b>	<b>Aitken</b>	<b>Accumulatio</b>	<b>Total Num.</b>
		(%)		( $10^3 \text{ cm}^{-3}$ )	( $10^3 \text{ cm}^{-3}$ )	n ( $10^3 \text{ cm}^{-3}$ )	( $10^3 \text{ cm}^{-3}$ )
<b>Summer</b>	Cluster 1	25	NW	2.9±1.7	6.3±3.8	4.0±1.8	13.2±5.3
	Cluster 2	12	N	4.8±2.8	5.0±4.4	1.2±0.7	10.9±6.6
	Cluster 3	51	SW	2.3±1.6	4.5±1.8	3.7±2.2	10.4±4.0
	Cluster 4	11	NE	2.4±1.1	3.6±1.9	2.0±1.2	8.0±3.1
<b>Winter</b>	Cluster 1	32	NW	3.3±2.4	7.4±3.1	5.9±4.0	16.7±6.8
	Cluster 2	19	N	3.4±2.3	4.6±4.3	1.2±0.8	9.3±6.5
	Cluster 3	23	SW	3.2±1.3	7.7±2.6	5.1±3.1	16.1±5.2
	Cluster 4	25	NW	3.6±1.7	7.1±3.0	4.5±3.4	15.2±6.1

476

477 During the summer campaign, the trajectory of cluster 3 from SW accounted for  
 478 the largest proportion of all trajectories (51%), which was followed by the NW cluster  
 479 1 (25%), N cluster 2 (12%) and NE cluster 4 (11%). The trajectory clusters are  
 480 dominated by cluster 1 and cluster 4 (NW), accounting for 32% and 25% in the winter.  
 481 Cluster 2 (N) and cluster 3 (SW) accounted for the remainder (19 and 23%,  
 482 respectively).

483 Figure 13 shows that the peak size of particle number size distributions during  
 484 summer was 70–80 nm, 50nm, 100nm, and 60-70nm for the trajectory cluster 1, 2, 3  
 485 and 4, respectively. The concentration of particles was highest for trajectory cluster 1  
 486 and lowest for trajectory cluster 4.



487

488 Figure 13. Box plots showing the particle number size distribution for the air back trajectory  
 489 clusters during the summer and winter: (a1, b1) Cluster 1, (a2, b2) Cluster 2, (a3, b3) Cluster 3,  
 490 (a4, b4) Cluster 4.

491 The Aitken mode and accumulation mode particles in cluster 1 during summer  
 492 had the highest number concentrations ( $6.3 \times 10^3 \text{ cm}^{-3}$  and  $4.0 \times 10^3 \text{ cm}^{-3}$ , respectively).  
 493 In contrast, trajectory cluster 2 had the highest number concentration of nucleation  
 494 mode particles ( $4.8 \times 10^3 \text{ cm}^{-3}$ ) and the lowest accumulation mode particles  
 495 ( $1.2 \times 10^3 \text{ cm}^{-3}$ ). The trajectory cluster 1 coming from the SW direction may carry  
 496 particles from the western urban areas into Beijing. The NPF event was the most  
 497 important contributor to the nucleation mode particles (Wang et al., 2011; Yue et al.,  
 498 2010; Zhang et al., 2011), and the concentration of the local background particles was  
 499 low under the control of the cluster 2 air mass, which facilitates the occurrence of  
 500 NPF events.

501 The peak size of particle number size distributions during winter was 110 nm,  
 502 40nm, 50-60nm, and 40-90nm for the trajectory cluster 1, 2, 3 and 4, respectively, as  
 503 shown in Fig.12. The concentration of particles was highest for trajectory cluster 1

504 and almost the same with the trajectory cluster 3 and 4, but the lowest for trajectory  
505 cluster 2. The Aitken mode and accumulation mode particles in cluster 2 during  
506 winter had the lowest number concentrations ( $4.6 \times 10^3 \text{ cm}^{-3}$  and  $1.2 \times 10^3 \text{ cm}^{-3}$ ,  
507 respectively). It was mainly because trajectory cluster 2 originated from a clean area  
508 with short transport pathways when compared with other clusters. However, the  
509 number concentrations of nucleation mode particles in all trajectory clusters were  
510 close to each other, indicating that there may be no obvious relationship between the  
511 occurrence of NPF and the source of air mass during winter.

512 The concentration of particles was highest for trajectory cluster 1 during both  
513 campaigns. Trajectory cluster 2 originated from northern clean areas and had a similar  
514 particle number size distribution during both winter and summer; however, the  
515 number concentrations of nucleation mode and Aitken mode particles in summer were  
516 slightly higher than those in winter. This may have occurred because of the high  
517 frequency of NPF events during summer, as well as the more active photochemical  
518 processes, which provided high concentrations ([Wang et al., 2014a](#); [Zhao et al., 2013](#))  
519 of low volatility condensable vapor molecules to further promote the condensation  
520 growth of nucleation mode particles. In addition, trajectory cluster 1, 4 and 3 in winter  
521 had different origins located in northwest and southwest Beijing, and the length of the  
522 trajectories differed, although the corresponding particle number size distributions  
523 was similar. A possible explanation for this is that the particle number size  
524 distributions in winter was greatly affected by local emissions ([Liu et al., 2016](#); [Tang  
525 et al., 2015](#); [Zheng et al., 2014](#)).

526

#### 527 **4. Summary and conclusions**

528 The particle number size distribution of aerosols (11.1 to 1083.3 nm) was  
529 monitored in Beijing during the HOPE-J<sup>3</sup>A field campaign. The average number  
530 concentration of particles during the summer and winter campaigns were  $9.6 \pm 4.8 \times 10^3$   
531  $\text{cm}^{-3}$  and  $13.9 \pm 8.3 \times 10^3 \text{ cm}^{-3}$ , respectively. There were frequent long-duration haze  
532 events during the winter campaign. The total number concentration of particles was

533 44.7% higher than that in the summer, with the largest difference being in Aitken  
534 mode particles. The number concentration of particles in Aitken mode dominated  
535 during both campaigns. Particle number concentrations showed close correlations  
536 with traffic and residents living activities and wind speed, especially for the  
537 nucleation mode and Aitken mode particles. The NPF events occurred more  
538 frequently and for a longer duration in summer. There is a shift in size distribution  
539 towards larger sizes when haze intensifies during the both campaigns. The analysis of  
540 trajectory cluster combined with meteorological conditions suggest that Aitken and  
541 accumulation mode particles were mainly from regional transport during the summer  
542 campaign, but from vehicle and coal-combustion emissions during the winter  
543 campaign.

544

## 545 **Acknowledgements**

546 This research was supported by the Natural Science Foundation of China  
547 (91544218), the National Key Research and Development Program of China  
548 (2016YFF0103004 and 2017YFC0209504), and the Science and Technological Fund  
549 of Anhui Province for Outstanding Youth (1808085J19). ZS is funded by UK Natural  
550 Environment Research Center (NE/N007190/1). The authors acknowledge Dr. Nan  
551 Ma and Dr. WanYun Xu for helping to draw the wind rose contour.

552

## 553 **References**

- 554 An, X., Zhu, T., Wang, Z., Li, C., Wang, Y., 2007. A modeling analysis of a heavy air pollution episode  
555 occurred in Beijing. *Atmospheric Chemistry & Physics* 7, 3103-3114.
- 556 Anderson, T.L., Charlson, R.J., Schwartz, S.E., Knutti, R., Boucher, O., Rodhe, H., Heintzenberg, J.,  
557 2003. Atmospheric science. Climate forcing by aerosol--a hazy picture. *Science* 300, 1103-1104.
- 558 Andreae, M., Rosenfeld, D., 2008. Aerosol--cloud--precipitation interactions. Part 1. The nature and  
559 sources of cloud-active aerosols. *Earth-Science Reviews* 89, 13-41.
- 560 Bahadur, R., Praveen, P.S., Xu, Y., Ramanathan, V., 2012. Solar absorption by elemental and brown  
561 carbon determined from spectral observations. *Proceedings of the National Academy of Sciences of*  
562 *the United States of America* 109, 17366-17371.
- 563 Cao, J.J., Chow, J.C., Lee, S.C., Watson, J.G., 2013. Evolution of PM<sub>2.5</sub> Measurements and Standards  
564 in the US and Future Perspectives for China. *Aerosol & Air Quality Research* 13, 1197-1211.
- 565 Chan, C.K., Yao, X., 2008. Air pollution in mega cities in China. *Atmospheric environment* 42, 1-42.

566 Chen, X., Wang, Z., Li, J., Chen, H., Hu, M., Yang, W., Wang, Z., Ge, B., Wang, D., 2017. Explaining  
567 the spatiotemporal variation of fine particle number concentrations over Beijing and surrounding  
568 areas in an air quality model with aerosol microphysics. *Environmental Pollution*, 1-12.

569 Cheung, H.C., Chou, C.C.K., Huang, W.R., Tsai, C.Y., 2013. Characterization of ultrafine particle  
570 number concentration and new particle formation in urban environment of Taipei, Taiwan.  
571 *Atmospheric Chemistry & Physics* 13, 8935-8946.

572 Gao, J., Chai, F., Wang, T., Wang, S., Wang, W., 2012. Particle number size distribution and new  
573 particle formation: New characteristics during the special pollution control period in Beijing.  
574 *Journal of Environmental Sciences* 24, 14-21.

575 Gao, J., Wang, T., Zhou, X., Wu, W., Wang, W., 2009. Measurement of aerosol number size  
576 distributions in the Yangtze River delta in China: Formation and growth of particles under polluted  
577 conditions. *Atmospheric Environment* 43, 829-836.

578 Han, L., Zhou, W., Li, W., 2015. Increasing impact of urban fine particles (PM<sub>2.5</sub>) on areas  
579 surrounding Chinese cities. *Scientific Reports* 5, 1-6.

580 Heim, M., Kasper, G., Reischl, G.P., Gerhart, C., 2004. Performance of a New Commercial Electrical  
581 Mobility Spectrometer. *Aerosol Sci. Technol.* 38, 3-14.

582 Huang, R.J., Zhang, Y., Bozzetti, C., Ho, K.F., Cao, J.J., Han, Y., Daellenbach, K.R., Slowik, J.G., Platt,  
583 S.M., Canonaco, F., 2014. High secondary aerosol contribution to particulate pollution during haze  
584 events in China. *Nature* 514, 218-222.

585 Huang, X., Wang, C., Peng, J., He, L., Cao, L., Qiao, Z., Jie, C., Wu, Z., Min, H., 2017.  
586 Characterization of particle number size distribution and new particle formation in Southern China.  
587 *Journal of Environmental Sciences* 51, 342-351.

588 Hussein, T., Puustinen, A., Aalto, P.P., Mäkelä, J.M., Hämeri, K., Kulmala, M., 2004. Urban aerosol  
589 number size distributions. *Atmospheric Chemistry and Physics* 4, 391-411.

590 Ji, D., Li, L., Wang, Y., Zhang, J., Cheng, M., Sun, Y., Liu, Z., Wang, L., Tang, G., Hu, B., 2014. The  
591 heaviest particulate air-pollution episodes occurred in northern China in January, 2013: Insights  
592 gained from observation. *Atmospheric Environment* 92, 546-556.

593 Joshi, M., Sapra, B., Khan, A., Tripathi, S., Shamjad, P., Gupta, T., Mayya, Y., 2012. Harmonisation of  
594 nanoparticle concentration measurements using GRIMM and TSI scanning mobility particle sizers.  
595 *Journal of Nanoparticle Research* 14, 1268.

596 Kulmala, M., 2003. How Particles Nucleate and Grow. *Science* 302, 1000-1001.

597 Kulmala, M., Kontkanen, J., Junninen, H., Lehtipalo, K., Manninen, H.E., Nieminen, T., Petäjä, T.,  
598 Sipilä, M., Schobesberger, S., Rantala, P., 2013. Direct observations of atmospheric aerosol  
599 nucleation. *Science* 339, 943-946.

600 Kulmala, M., Riipinen, I., Sipilä, M., Manninen, H.E., Petäjä, T., Junninen, H., Maso, M.D., Mordas, G.,  
601 Mirme, A., Vana, M., 2007. Toward direct measurement of atmospheric nucleation. *Science* 318,  
602 89-92.

603 Lehtinen, K., Korhonen, H., Maso, M.D., Al, E., 2003. On the concept of condensation sink diameter.  
604 *Boreal Environment Research* 8, 405-411.

605 Liang, P., Zhu, T., Fang, Y., Li, Y., Han, Y., Wu, Y., Hu, M., Wang, J., 2017. The Role of Meteorological  
606 Conditions and Pollution Control Strategies in Reducing Air Pollution in Beijing during APEC  
607 2014 and Parade 2015. *Atmospheric Chemistry & Physics*, 1-62.

608 Liu, Z., Hu, B., Zhang, J., Xin, J., Wu, F., Gao, W., Wang, M., Wang, Y., 2017. Characterization of fine  
609 particles during the 2014 Asia-Pacific economic cooperation summit: Number concentration, size

610 distribution and sources. *Tellus Series B-chemical & Physical Meteorology* 69, 1303228.

611 Liu, Z., Wang, Y., Bo, H., Ji, D., Zhang, J., Wu, F., Xin, W., Wang, Y., 2016. Source appointment of fine  
612 particle number and volume concentration during severe haze pollution in Beijing in January 2013.  
613 *Environmental Science & Pollution Research International* 23, 6845-6860.

614 Mahowald, N., 2011. Aerosol indirect effect on biogeochemical cycles and climate. *Science* 334,  
615 794-796.

616 Nel, A., 2005. Air pollution-related illness: effects of particles. *Science* 308, 804-806.

617 Parrish, D.D., Zhu, T., 2009. Clean air for megacities. *Science* 326, 674-675.

618 Pirjola, L., Kulmala, M., Wilck, M., Bischoff, A., Stratmann, F., Otto, E., 1999. Formation of Sulphuric  
619 Acid Aerosols and Cloud Condensation Nucleation: an Expression for Significant Nucleation and  
620 Model Comparison. *J. Aerosol Sci.* 30, 1079-1094.

621 Quan, J., Tie, X., Zhang, Q., Liu, Q., Li, X., Gao, Y., Zhao, D., 2014. Characteristics of heavy aerosol  
622 pollution during the 2012–2013 winter in Beijing, China. *Atmospheric Environment* 88, 83-89.

623 Ramanathan, V., Crutzen, P.J., Kiehl, J.T., Rosenfeld, D., 2001. Aerosols, climate, and the hydrological  
624 cycle. *Science* 294, 2119.

625 Reischl, G.P., 1991. Measurement of Ambient Aerosols by the Differential Mobility Analyzer Method:  
626 Concepts and Realization Criteria for the Size Range Between 2 and 500 nm. *Aerosol Sci. Technol.*  
627 14, 5-24.

628 Schäfer, K., Wang, Y., Norra, S., Shen, R., Xin, J., Ling, H., Tang, G., Münkel, C., Schleicher, N., Yu, Y.,  
629 2013. Meteorological Influences Within the Context of Air Quality in Beijing.

630 Shen, X., Sun, J., Zhang, Y., Wehner, B., Nowak, A., Tuch, T., Zhang, X., Wang, T., Zhou, H., Zhang,  
631 X., 2011. First long-term study of particle number size distributions and new particle formation  
632 events of regional aerosol in the North China Plain. *Atmospheric Chemistry and Physics* 11,  
633 1565-1580.

634 Shi, Z.-b., He, K.-b., YU, X.-c., YAO, Z.-l., YANG, F.-m., Rui, M., JIA, Y.-t., ZHANG, J., 2007.  
635 Diurnal variation of number concentration and size distribution of ultrafine particles in the urban  
636 atmosphere of Beijing in winter. *Journal of Environmental Sciences* 19, 933-938.

637 Stanier, C.O., Khlystov, A.Y., Pandis, S.N., 2004. Nucleation events during the Pittsburgh Air Quality  
638 Study: description and relation to key meteorological, gas phase, and aerosol parameters special  
639 issue of aerosol science and technology on findings from the fine particulate matter supersites  
640 program. *Aerosol Sci. Technol.* 38, 253-264.

641 Sun, Y., Jiang, Q., Wang, Z., Fu, P., Li, J., Yang, T., Yin, Y., 2014. Investigation of the sources and  
642 evolution processes of severe haze pollution in Beijing in January 2013. *Journal of Geophysical*  
643 *Research: Atmospheres* 119, 4380-4398.

644 Sun, Y., Wang, Z., Wild, O., Xu, W., Chen, C., Fu, P., Wei, D., Zhou, L., Zhang, Q., Han, T., 2016.  
645 “APEC Blue”: Secondary Aerosol Reductions from Emission Controls in Beijing. *Scientific*  
646 *Reports* 6, 20668.

647 Sun, Y.L., Wang, Z.F., Du, W., Zhang, Q., Wang, Q.Q., Fu, P.Q., Pan, X.L., Li, J., Jayne, J., Worsnop,  
648 D.R., 2015. Long-term real-time measurements of aerosol particle composition in Beijing, China:  
649 seasonal variations, meteorological effects, and source analysis. *Atmospheric Chemistry & Physics*  
650 15, 10149-10165.

651 Tang, G., Zhao, P., Wang, Y., Gao, W., Cheng, M., Xin, J., Li, X., Wang, Y., 2017. Mortality and air  
652 pollution in Beijing: The long-term relationship. *Atmospheric Environment* 150, 238-243.

653 Tang, G., Zhu, X., Hu, B., Xin, J., Wang, L., Münkel, C., Mao, G., Wang, Y., 2015. Impact of emission



654 controls on air quality in Beijing during APEC 2014: lidar ceilometer observations. *Atmospheric*  
655 *Chemistry & Physics* 15, 12667-12680.

656 Wang, D., Guo, H., Cheung, K., Gan, F., 2014a. Observation of nucleation mode particle burst and new  
657 particle formation events at an urban site in Hong Kong. *Atmospheric Environment* 99, 196-205.

658 Wang, T., Nie, W., Gao, J., Xue, L.K., Gao, X.M., Wang, X.F., Qiu, J., Poon, C.N., Meinardi, S., Blake,  
659 D., 2010. Air quality during the 2008 Beijing Olympics: Secondary pollutants and regional impact.  
660 *Atmospheric Chemistry & Physics* 10, 7603-7615.

661 Wang, X., Chen, J., Cheng, T., Zhang, R., Wang, X., 2014b. Particle number concentration, size  
662 distribution and chemical composition during haze and photochemical smog episodes in Shanghai.  
663 *Journal of Environmental Sciences* 26, 1894-1902.

664 Wang, Z., Hu, M., Sun, J., Wu, Z., Yue, D., Shen, X., Zhang, Y., Pei, X., Cheng, Y., Wiedensohler, A.,  
665 2013. Characteristics of regional new particle formation in urban and regional background  
666 environments in the North China Plain. *Atmospheric Chemistry and Physics* 13, 12495-12506.

667 Wang, Z.B., Hu, M., Yue, D.L., Zheng, J., Zhang, R.Y., Wiedensohler, A., Wu, Z.J., Nieminen, T., Boy,  
668 M., 2011. Evaluation on the role of sulfuric acid in the mechanisms of new particle formation for  
669 Beijing case. *Atmospheric Chemistry & Physics* 11, 24165-24189.

670 Wang, Z.B., Hu, M., Zeng, L.W., Xue, L., He, L.Y., Huang, X.F., Zhu, T., 2014c. Measurements of  
671 particle number size distributions and optical properties in urban Shanghai during 2010 World Expo:  
672 relation to air mass history. *Tellus Series B-chemical & Physical Meteorology* 66, 1175-1176.

673 Watson, J.G., 2002. Visibility: Science and regulation. *Journal of the Air & Waste Management*  
674 *Association* 52, 628-713.

675 Wehner, B., Wiedensohler, A., 2003. Long term measurements of submicrometer urban aerosols:  
676 statistical analysis for correlations with meteorological conditions and trace gases. *Atmospheric*  
677 *Chemistry and Physics* 3, 867-879.

678 Wu, Z., Hu, M., Lin, P., Liu, S., Wehner, B., Wiedensohler, A., 2008. Particle number size distribution  
679 in the urban atmosphere of Beijing, China. *Atmospheric Environment* 42, 7967-7980.

680 Wu, Z., Hu, M., Liu, S., Wehner, B., Bauer, S., Blling, A.M., Wiedensohler, A., Petäjä, T., Maso, M.D.,  
681 Kulmala, M., 2007. New particle formation in Beijing, China: Statistical analysis of a 1 - year data  
682 set. *Journal of Geophysical Research Atmospheres* 112, D09209.

683 Wu, Z., Zheng, J., Shang, D., Du, Z., Wu, Y., Zeng, L., Wiedensohler, A., Hu, M., 2016. Particle  
684 hygroscopicity and its link to chemical composition in the urban atmosphere of Beijing, China,  
685 during summertime. *Atmospheric Chemistry and Physics* 16, 1123-1138.

686 Xin, J.Y., Wang, Y.S., Tang, G.Q., Wang, L.L., Yang, S., Wang, Y.H., Hu, B., Song, T., Ji, D.S., Wang,  
687 W.F., 2010. Variability and reduction of atmospheric pollutants in Beijing and its surrounding area  
688 during the Beijing 2008 Olympic Games. *Chinese Science Bulletin* 55, 1937-1944.

689 Xu, R., Tang, G., Wang, Y., Tie, X., 2016a. Analysis of a long-term measurement of air pollutants  
690 (2007–2011) in North China Plain (NCP); Impact of emission reduction during the Beijing  
691 Olympic Games. *Chemosphere* 159, 647-658.

692 Xu, X., Zhao, W., Zhang, Q., Wang, S., Fang, B., Chen, W., Venables, D.S., Wang, X., Pu, W., Wang,  
693 X., 2016b. Optical properties of atmospheric fine particles near Beijing during the HOPE-J3A  
694 campaign. *Atmospheric Chemistry & Physics* 16, 6421-6439.

695 Yue, D., Hu, M., Wu, Z., Wang, Z., Guo, S., Wehner, B., Nowak, A., Achtert, P., Wiedensohler, A., Jung,  
696 J., 2009. Characteristics of aerosol size distributions and new particle formation in the summer in  
697 Beijing. *Journal of Geophysical Research Atmospheres* 114, 1159-1171.

698 Yue, D.L., Hu, M., Zhang, R.Y., Wang, Z.B., 2010. The roles of sulfuric acid in new particle formation  
699 and growth in the mega-city of Beijing. *Atmospheric Chemistry & Physics Discussions* 10,  
700 4953-4960.

701 Zhang, H., Hu, D., Chen, J., Ye, X., Wang, S.X., Hao, J.M., Wang, L., Zhang, R., An, Z., 2011. Particle  
702 Size Distribution and Polycyclic Aromatic Hydrocarbons Emissions from Agricultural Crop  
703 Residue Burning. *Environmental Science & Technology* 45, 5477-5482.

704 Zhang, J., Chen, Z., Lu, Y., Gui, H., Liu, J., Liu, W., Wang, J., Yu, T., Cheng, Y., Chen, Y., 2017.  
705 Characteristics of aerosol size distribution and vertical backscattering coefficient profile during  
706 2014 APEC in Beijing. *Atmospheric Environment* 148, 30-41.

707 Zhang, R., Jing, J., Tao, J., Hsu, S.C., 2013. Chemical characterization and source apportionment of  
708 PM<sub>2.5</sub> in Beijing: seasonal perspective. *Atmospheric Chemistry & Physics* 13, 7053-7074.

709 Zhang, X., Zhang, Y., Sun, J., Zheng, X., Li, G., Deng, Z., 2016. Characterization of particle number  
710 size distribution and new particle formation in an urban environment in Lanzhou, China. *J. Aerosol*  
711 *Sci.* 103, 53-66.

712 Zhao, X., Zhao, P., Xu, J., Meng, W., Pu, W., Dong, F., He, D., Shi, Q., 2013. Analysis of a winter  
713 regional haze event and its formation mechanism in the North China Plain. *Atmospheric Chemistry*  
714 *and Physics* 13, 5685-5696.

715 Zheng, S., Pozzer, A., Cao, C.X., Lelieveld, J., 2014. Long-term (2001-2012) fine particulate matter  
716 (PM<sub>2.5</sub>) and the impact on human health in Beijing, China. *Atmospheric Chemistry & Physics*  
717 *Discussions* 14, 5715-5725.

718 Zhu, X., Tang, G., Hu, B., Wang, L., Xin, J., Zhang, J., Liu, Z., Munkel, C., Wang, Y., 2016. Regional  
719 pollution and its formation mechanism over North China Plain: A case study with ceilometer  
720 observations and model simulations. *Journal of Geophysical Research Atmospheres* 121, 1-15.

721 Zhuang, X., Wang, Y., He, H., Liu, J., Wang, X., Zhu, T., Ge, M., Zhou, J., Tang, G., Ma, J., 2014. Haze  
722 insights and mitigation in China: An overview. *Journal of Environmental Sciences* 26, 2-12.

723